Three-Dimensional Computational Modeling of the Detonation of a Barricaded Munitions Stack Within a Temporary Munitions Storage Area

Richard E. Lottero
U.S. Army Research Laboratory
Weapons and Materials Research Directorate
Aberdeen Proving Ground, MD 21005-5066

DOD HPCMP 2001 Users Group Conference
Biloxi, MS
18–21 June 2001

This paper describes the results of three-dimensional (3-D) hydrocode computations performed at the Major Shared Resource Center (MSRC) operated by the U.S. Army Research Laboratory (ARL) at its Aberdeen Proving Ground, MD location. This site is one of four MSRCs established under the DoD High Performance Computing Modernization Program (HPCMP). The 3-D computations described herein were performed during the pioneer mode on the new 512-processor International Business Machines SP Power3. Each of the 3-D computations utilized 120 processors operating in parallel, together modeling the detonation of a donor munitions stack and the loading on and response of a protective water barricade and a nearby acceptor munitions stack. The computations were done with the CTH hydrocode, developed by the Sandia National Laboratories and supported on the ARL MSRC site under the HPCMP. The computations were performed as one part of a study by ARL titled "Munitions Survivability Technology" in support of the U.S. Army Defense Ammunition Logistics Activity. The overall goal of the study was to suppress the propagation of fire and explosion between stacks of munitions in a field-expedient storage area through the use of barricades between, and protective coverings on, the stacks.

The first 3-D computation was fully coupled, with the detonating donor stack, the barricade, and the acceptor stack munitions stack all simulated in the flow field. Numerical instabilities forced a stoppage of the computation before the loading cycle on the acceptor stack was complete. A second 3-D computation that included only the barricade and acceptor stack, each assigned initial translational velocities

equal to those from the first 3-D computation, was run through nearly all of the loading cycle on the acceptor stack, at which time it also stopped because of numerical instabilities. The results of these combined 3-D computations are compared with those from earlier two-dimensional (2-D) computations for the same geometry. The 2-D computations were run earlier in serial mode on other computers at the same ARL MSRC site. The protection provided by the barricade to the acceptor stack and the blast and impact loading on the acceptor stack were the dynamic parameters of principal interest.

INTRODUCTION

This report documents the results of an extension into three-dimensional (3-D) modeling from previous two-dimensional (2-D) studies reported by the author of the detonation of a munitions stack in a field-expedient munitions storage area. During normal peace-time operations in secure areas, munitions are stored in accordance with requirements and guidelines set forth in Army Regulation 385-64 (AR-385-64). AR-385-64 includes the relevant Department of Defense Explosives Safety Board (DDESB) requirements and guidelines [1]. When Army units must operate in combat or contingency situations, it is typically not possible to follow these standard guidelines. Chapter 10, "Theater of Operations Quantity Distance," [1] provides guidelines for these situations. Chapter 10 was deemed to have deficiencies after a comprehensive review by a DDESB working group in February, 1997. A new version of Chapter 10 was recommended in 1998. The differences are summarized by O'Heran [2].

A continuing problem for the U.S. Army has been to find ways to prevent chain reactions from occurring in field-expedient munitions storage areas. When some initiating event occurs in a stack of munitions, chain reactions can subsequently occur in nearby stacks of munitions. The munitions stack that experiences the first initiating event is hereinafter referred to as the "donor" stack. A munitions stack that is in proximity to a donor stack is referred to as an "acceptor" stack. Any munition within such a stack is referred to as an "acceptor" munition, or simply as an "acceptor." Often, the result is that much or all of the supply of munitions and other materiel in the storage area is lost. The chain reaction can propagate by a variety of means. Some of the means are (a) relatively immediate sympathetic detonation caused by impact or shock, and (b) somewhat slower initiations caused by such events as crushing at high strain rates, fragment impact and penetration, and fire. Not all of the relatively prompt (i.e., within milliseconds) impact-related mechanisms for causing a true high-order detonation are well understood and are a matter of continuing debate. The criteria for direct

initiation of detonation by shock overpressure are relatively well known. An excellent discussion of direct shock initiation of explosives is presented in a report by Liddiard and Forbes [3]. The major findings of that report are that the modified gap test (MGT) [4] indicates that the "...onset of detectable burning occurs at peak stresses in explosives of 8.8 to 75.0 kbar in the explosives that have been tested..." The underwater shock test (UST) [4] indicates that "...burning occurs at peak stresses of 4 to 12 kbar in the e
statement is made [3] that "...compression by a 3- or 4-kbar shock is, of itself, a sufficient external stimulus to start chemical reaction in a heterogeneous solid explosive such as pentolite."

The criteria for predicting the initiation of explosives, through either relatively prompt high-order detonation or a much slower burning process by an event dominated by mechanical shearing are not as well understood, and are a matter of continuing debate. Liddiard and Forbes [3] also presented a brief discussion of shear initiation of explosives, including a table that shows the threshold of burning for various explosives for combinations of lateral "...flow rates of 28 45 m/s resulting from shock pressures in water of 3-6 kbar." These shock pressures, when combined with lateral flow, are generally lower for a given explosive than the shock pressures for simple shock initiation. Here, lateral flow refers to flow induced in the explosive in a normal direction to the shock velocity vector. In a material that can support viscous and other deviatoric stresses, the lateral flow is reasonably related to and is an indicator of shearing stresses and the strain rate in that normal direction.

The computations reported herein constitute one part of a now-ended U.S. Army Research Laboratory (ARL) project, "Munitions Survivability Technology," supported and funded by the U.S. Army Defense Ammunition Logistics (Ammolog) Activity. Earlier computational work on this project, which has been completed and reported, focused on evaluating the blast from the complete high-order detonation of a simplified donor munitions stack modeled as a bare charge, the loading on and response of various intervening barricades, and the subsequent loading on and response of an acceptor munitions stack, all within a 2-D flow field. The first ARL report [5] documented a pair of uncoupled hydrodynamics computer code ("hydrocode") computations that used a 1996 version of the CTH [6] hydrocode. (Please see the CTHGEN users' manual [7] for grid generation and the CTH users' manual [8] for running the CTH hydrocode.) Both the donor and acceptor munitions stacks were simplified versions of stacks of 72 pallets each of M107 155-mm munitions [9]. The choice of the munitions stack configuration for those and all subsequent computations for munitions stacks to this time was based on earlier ARL work on fragmentation propagation [10]. The donor stack was modeled here and in all similar computations as a bare explosive charge with a nominal mass of 4,000 kg of Composition B (hereinafter referred to as "Comp-B"). The term "uncoupled" is used here in a specific mathematical sense.

The first attempts to run a single, fully coupled computation resulted in failures because of numerical stability problems. This and all previous computations attempted to include the detonation of the donor stack, the loading and response of the barricade, the impact of the barricade in its distorted form against the acceptor stack, and the loading and response of the acceptor stack in a single simulation. Because of the failures, the problem was divided into two uncoupled computations. Using simplified representations of the stack and barricade in a 2-D Cartesian coordinates system, the first of the two uncoupled computations in that report [5] simulated the detonation of the donor stack, the loading on a water barricade, and the ensuing bulk motion of the water barricade. Performing computations in a 2-D Cartesian coordinates system implies that any resulting distortion of the barricade up to actual breakup would be in a "plane-strain" mode. The water barricade shape being evaluated was based on a design provided to Ammolog by one of its contractors [11]. A simplified trapezoidal cross section for the water barricade was assumed, with the sloping sides having a 30-degree included angle to a line perpendicular to the ground plane. The separation distance, i.e., the "standoff distance," measured along the ground plane between a presumed right face of the donor stack and the left-most edge at the bottom of the water barricade was 3.05 m (10.0 ft). The 3.05-m standoff was identified by Ammolog and its consultants as a probable first estimate of the standoff distance that might be chosen for field use in the absence of any new technical guidance. The second of the two uncoupled computations simulated the water barricade, reformed into its original undistorted shape, traveling toward the acceptor stack at the final bulk velocity from the first computation and impacting the acceptor stack. This provided insight into the peak pressures and integrated blast and impact loading on the acceptor stack and its whole-body response to that loading. However, the effect of the decoupling on the loading on and response of the acceptor stack could not be quantified in that report. This work was also summarized in a technical paper [12].

A later version of CTH [6] (this is still the basic reference), along with the complementary documentation and instructions for the grid generation [13] and CTH hydrocode [14] input options and execution instructions, was used to run the first of three series of fully coupled computations [15]. These 2-D Cartesian computations simulated the same donor and acceptor stacks and trapezoidal water barricade as were simulated in the previous study [5]. Five computations were completed, each for a different standoff distance. The standoff distances in each computation were kept equal between both the donor stack and the barricade on one side and the barricade and the acceptor stack on the other side. These standoff distances were 2.00 m, 2.25 m, 2.50 m, 2.75 m, and 3.05 m. This version of CTH had better numerical stability than the previous version, so it was possible in each of the five computations to run the problems in a fully coupled mode. The essential difference is that the impact of the barricade on the acceptor stack for the computation for the 3.05-m standoff in this series had the barricade striking as a

distorted and differentially accelerated mass rather than as a reshaped mass with a uniform bulk velocity as was done in the second of the two uncoupled computations [5]. One of the primary points of information from this first series of computations was that there is a disproportionately small increase as an inverse function of standoff distance in loading on and bulk acceleration of the acceptor stack over this 2.00- to 3.05-m range in standoff distances. This indicated that there may be only a moderate penalty in increased loading on the acceptor stack in this simplified simulation for a relatively large reduction in required land area for at least a field-expedient, temporary munitions storage site. The sloping sides of the trapezoidal water barricade also helped to develop shear layers in the flow that kept explosive products from impinging on the acceptor stack during all of the nominal 40-ms simulation times by directing them upward.

The second series of fully coupled computations simulated the same donor and acceptor munitions stacks separated by a water barricade with a thin (1.17-m width) rectangular cross section [16]. Three standoff distances (2.00 m, 2.50 m, and 3.05 m) were simulated to match three of the previously simulated distances and cover the same range. It was noted in that report [16] that changing from the trapezoidal cross section to the rectangular for a given standoff had the effect, which is probably undesired, of moving the center of mass of the barricade closer to the donor stack. The thin rectangular barricade also had a significantly smaller mass per unit depth (28.6 kg/cm) in the 2-D Cartesian computational flow field than did the trapezoidal cross section barricade, which had 58.7 kg/cm of depth. Comparisons with the previously reported computations for the water barricade with the trapezoidal cross section showed that the barricade-impact loading on the acceptor stack was much greater at a given standoff for the thin rectangular barricade. This was shown to be primarily because of a combination of the greater efficiency of the vertical sides of the thin rectangular barricade in accumulating greater loading in both peak values of pressure and total integrated impulse from the detonation of the donor stack, the lower mass of that barricade, and the greater efficiency of its vertical opposite side in delivering loading to the acceptor stack. Considerable amounts of explosive products impinged directly on the acceptor stack at later time for all of the computations for the thin rectangular water barricade, which was also disintegrated and swept out of the flow field much more quickly than was the case for the trapezoidal barricade.

The third series of fully coupled computations simulated the same configurations as for the thin rectangular water barricade, except that in these, the water barricade thickness was 1.70 m. The mass of that water barricade was 41.5 kg/cm of depth. These computations were reported [17, 18] along with a summary analysis that included all of the results from the three series of fully coupled computations. A simple correlation was presented that related the final values of the total integrated impulse on the side of the acceptor stack facing the barricade for all computations with a scaled barricade mass. This scaled barricade mass was

computed from a combination of the actual barricade mass per centimeter of depth, a trigonometric function for the slope of each of the two sides of the barricade, and a 1/3 power of the standoff distance.

Several years ago, a series of experiments [19] was performed at ARL with the goal of identifying at least some of the worst-case acceptors among munitions by subjecting several different types of munitions to either double impact or crushing impact from a steel flyer plate. Double impact occurs when a round is struck on one side, is thereby accelerated, and then strikes another independent object. That other object could be anything, including another munition. Crushing impact occurs when a heavy object strikes buffering material on one side of a munition that is already in contact with another munition or hard object on its opposite side. Two of the munitions that were identified in that study as candidates to be considered as probable worst-case acceptors for either double or crushing impact are the M2A3 demolition charge and the M483 155-mm projectile. Two series of CTH [6] computations were performed which matched representative subsets of double-impact and crushing-impact experiments from that study [19]. These computations have also been reported [20, 21], with the finding that the various exothermic reactions that were observed were most likely not caused by direct shock. The possibility that they were shear-initiation events was suggested.

The computations discussed herein are 3-D CTH [6] computations of a donor stack, a trapezoidal water barricade, and an acceptor stack in a postulated field-expedient munitions storage area. A 3.05-m standoff distance is assumed between both the donor stack and the water barricade and between the water barricade and the acceptor stack. As before, the standoff distance is measured along the ground plane between the bases of the munition stacks and the appropriate face of the water barricade. The layout and dimensions used in the 3-D computations are based on a combination of those used in the earlier 2-D computations [5, 15] and a full-scale experiment performed at China Lake, CA [22] for ARL on behalf of Ammolog.

THE FULL-SCALE EXPERIMENTAL WORK

The experiment [22] of direct interest in this report consisted of a symmetric arrangement of a central donor stack, a water-bag barricade on each side, and an acceptor stack on the far side of each water barricade. The water-bag barricades were provided by Federal Fabrics-Fibers, Inc., under contract [11] to Ammolog. The barricade was constructed on site as a pyramid of three bags, each of which was nominally 1.372 m (54 in) in diameter and 7.01 m (23 ft) long. The donor stack consisted of 576 M105 155-mm projectiles, each of which contained 6.98 kg (15.4 lbm) of Comp-B explosive. Its approximate dimensions were 2.06 m (6.75 ft) in depth (i.e., the coordinate direction moving from the donor stack to the barricade and then to the acceptor stack), 4.13 m (13.55 ft) in length, and 1.58 m

(5.20 ft) in height. It was detonated by a command detonation of 16 centrally located projectiles. The side of each acceptor stack facing its protective water barricade was composed of several of the most sensitive munitions: "M2 hole diggers, M864 Rocket Assisted Projectile (RAP) rounds (unfuzed bomblets), M67 hand grenades (unfuzed), and M203 propelling charges. These charges were backed up with stacked pallets of M107 projectiles" [22]. The standoff distance was 3.05 m (10.0 ft). One acceptor stack detonated after a relatively long delay, the exact value of which is uncertain. The other did not. During that delay, the acceptor stack that detonated slid along the ground for an undetermined but considerable distance.

SUMMARY OF CTH HYDROCODE COMPUTATIONS

Three-Dimensional Computations

The 3-D computations reported herein were performed with the CTH [6, 13, 14] hydrocode. Although not originally planned, it was necessary to perform two uncoupled 3-D computations. The first of the two 3-D computations was intended to simulate the entire, fully coupled detonation and interaction event, starting with the detonation of the donor stack and proceeding to the end of the loading on the left face of the acceptor stack. It is designated herein as computation 3DC, with the "3D" indicating a 3-D computation and "C" indicating that the fully coupled computational flow field contains the donor stack, the barricade, and the acceptor stack.

Computation 3DC was run for a simulated time from 0.00 to 47.40 ms. Figure 1 shows a 2-D plane in the X (left to right) and Z (vertical) directions for 3DC at time = 0.00. This plane is cut through the flow field at the first set of active computational cells in the Y direction, so it is an elevation view. The flow field is bounded on the left (X = 0.00) by a reflective symmetry plane, appearing edge-on in Figure 1 as the Z axis. The right boundary of the flow field is an outflow-only transmissive boundary, appearing as the right-most edge of the yellow color at X = 16.32 m. The yellow color denotes the simulated atmospheric air. The bottom boundary of the flow field is a reflecting plane that simulates the ground surface at Z = 0.00. The top boundary of the flow field is an outflow-only transmissive boundary, appearing as the top-most edge of the yellow color at Z = 9.01 m. The measure of depth of the flow field (parallel to the left and right surfaces of the stacks and barricade) is in the Y direction, with a positive Y vector coming out of the page in a normal direction. The boundary at Y = 0.00 is a reflective symmetry plane, and the boundary at Y = 7.01 m is an outflow-only transmissive boundary.

The red rectangle suspended above the bottom boundary and in contact with the left boundary is a bare charge of Comp-B representing the full explosive mass, 4,000 kg, in the donor stack. It is modeled as a solid rectangle of unreacted

Comp-B at its reference density [23] of 1.72 g/cm3. The explosive charge representing the donor stack was initiated at its true geometric center, the point (X = 0.0, Y = 0.0, Z = 1.2192 m), taking into account the existence of its two symmetry planes in this simulation. The "programmed burn" model [24] was used to propagate the detonation. The blue trapezoid represents the cross section of the water [25] barricade. The black (iron) rectangle represents the cross section of the acceptor stack, modeled as a solid-iron rectangular parallelepiped. This allowed a reasonably accurate computation of its momentum as a function of time, which was later used with the correct mass value to produce the X-direction velocity of a presumed monolithic acceptor stack. Figure 2 shows a plan view of the computational flow field at time = 0.00, consisting of a cut along an X-Y plane in the first active flow field cells in the Z direction. The boundaries of the yellow color denote the limits of flow field.

At time = 0.00, all materials in the flow field were at rest and at a pressure of one atmosphere. Computation 3DC was stopped at 47.40 ms because the computed time step for the next pass through the grid fell below a minimum acceptable value required for continuing the computation. This appeared to be related to the numerical instabilities in the simulated acceptor stack, which will be discussed later in this report. Numerous attempts to get the computation to proceed beyond this point in time failed. An elevation view of the flow field at 47.40 ms is shown in Figure 3, and a plan view is shown in Figure 4. The impact of the translating water barricade on the left surface of the acceptor stack was in its early stages at this time.

At this point, the decision was made to continue the simulation with a second, uncoupled computation. This uncoupled 3-D computation, designated herein as 3DU, was set up in the same manner as was the second uncoupled 2-D computation reported previously [5]. The designation "3DU" signifies that this 3-D computation included only the barricade and the acceptor stack, with no inclusion of the donor stack. Figure 5 shows an elevation view the computational flow field for 3DU at its starting time of 47.40 ms, and Figure 6 shows a plan view. The water barricade has been reconstituted into a slight variation of its original trapezoidal cross sectional shape. The original height of 2.4384 m has been preserved, as has the 30-degree angle from the vertical of the sloping sides. Because some of the mass of the water barricade had flowed out of the computational flow field in 3DC, the width in the X direction of the rectangular core of the barricade was reduced to 90.66 cm from the original 1.00 m to account for this. The barricade was assigned a bulk velocity in the positive X direction of 45.72 m/s, the ending-time bulk X-direction velocity of the water in computation 3DC. The acceptor stack was modeled as a massive, solid iron rectangular parallelepiped in the same way as for 3DC. It was given an initial velocity of 1.72

m/s, the value of the velocity of the massive acceptor stack at 47.40 ms in 3DC. Thus, the X-direction momenta of both the water barricade and the acceptor stack were preserved from one computation to the next.

Computation 3DU was run from its (non-zero) initial time of 47.40 ms until it also halted because of numerical instabilities at 131.74 ms. Difficulties were experienced in trying to extend the computation beyond that time. Analysis of the results indicated that the loading on the left surface of the acceptor stack had essentially ended by that time. A decision to complete the analysis and report the results was made. An elevation view of the flow field at 131.74 ms is shown in Figure 7, and a plan view is shown in Figure 8.

Two-Dimensional Computations

To facilitate the comparison of the 3-D computational results to the earlier 2-D results [5, 15], representative plots from the previously reported 2-D computations are shown here. Two representative plots from the fully coupled 2-D computation for the trapezoidal water barricade at a 3.05-m standoff [15] are shown. The designation in that report [15] was "980505," but hereinafter it will be designated as 2DC to be consistent with the 3-D nomenclature used here. Figure 9 shows the computational flow field for 2DC at time = 0.00, the start of the computation. This looks essentially the same as the elevation view for 3DC shown in Figure 1. Figure 10 shows the flow field for 2DC at its ending time of 40.00 ms.

The first report on 2-D computations [5] described the results of two separate computations simulating the detonation of the donor stack and the subsequent dynamic interaction of the blast field with the trapezoidal water barricade and the acceptor stack. The standoff distance in these computations was 3.05 m. The first of those two computations was designated in that report as computation "970908." It was intended to be a fully coupled computation which would proceed from the initiation of the donor stack through the completion of the loading phase on the acceptor stack. For purposes of this report and to use consistent notation, this computation will hereinafter be referred to as computation 2DUa. Even though this computation is fully coupled, the "Ua" designation indicates that it is one computation of an uncoupled pair. The computational flow field for 2DUa at time = 0.00, the start of the computation, is shown in Figure 11. Numerical instabilities forced a premature halt of 2DUa at 8.00 ms of simulated time, well before the translating and distorted water barricade could interact with the acceptor stack. The flow field at time = 8.00 ms is shown in Figure 12.

After several attempts to continue computation 2DUa beyond 8.00 ms failed, a second uncoupled computation, originally designated [5] as "971001," was set up with just the water barricade and a solid iron rectangle representing the acceptor

stack. The computational flow field for 2DUb, the nomenclature for that computation for this report, at its starting time = 0.00 is shown in Figure 13. The water barricade was reconstituted into its original mass per unit depth and trapezoidal shape and assigned an X-direction velocity equal to that of the bulk velocity in that direction of the distorted water barricade in 2DUa. The acceptor stack was modeled as a solid rectangle of iron with the original height of the acceptor stack in 2DUa, a thickness such that its mass per unit depth was the same as an actual acceptor stack, and with no initial X-direction velocity. The X-direction velocity of the corrected-mass acceptor stack at the ending time of 2DUa was negligible because the only loading on it to that point in time was the relatively weak air shock. Computation 2DUb was run from its assigned starting time = 0.00 until a simulated time of 7.80 ms, at which time halted because of numerical instabilities. The flow field at 7.80 ms is shown in Figure 14. The loading phase on the left surface of the acceptor stack had essentially ended by that time.

ANALYSIS OF RESULTS

Barricade Dynamics

The barricade X-direction velocity for the various computations is shown in Figure 15. The velocity of the barricade in computation 3DC is shown by the black line, plotted from 0.00 to 47.40 ms. It indicates a peak value of 49.63 m/s at 7.15 ms. The velocity for 3DU is shown by the dark blue line, plotted from an assigned initial value of 45.72 m/s at 47.40 ms to the ending time of 131.74 ms. As would be expected, there is a monotonic decrease in X-direction velocity for 3DU with time. For comparison, the X-direction velocity from the fully coupled 2-D computation, 2DC, is plotted with a cyan line from 0.00 to 40.00 ms. It shows a peak velocity of 178.2 m/s at 10.93 ms. The peak velocity in 2DC is 3.6 times greater that that for the peak in 3DC. This difference is entirely because of the addition of the third dimension for flow-field effects and including the actual finite dimensions of the donor stack, barricade, and acceptor stack in that direction. For comparison, the results for computations 2DUa and 2DUb are also shown in Figure 15 as two disjoint green lines, with a gap of 28.12 ms between the end of the line for 2DUa and the beginning of the line for 2DUb. This gap of 28.12 ms is the estimated time shift needed to correlate the results from 2DUb with the late-time results from 2DC [15]. The peak X-direction bulk velocity for the water barricade in 2DUa at its ending time is 173.4 m/s, which compares well with the peak velocity of 178.2 m/s found in 2DC. This at least implies that the necessary decoupling of the 3-D computations probably did not result in a great error in determining the peak bulk velocity of the water barricade.

Figure 16 shows the acceleration histories of the water barricade for the same set of computations. Computation 3DC has a single early peak of 56.28 km/s2 at 1.19 ms and no other significant accelerations, either positive or negative, in the plotting scale of Figure 16. Computation 3DU shows no significant accelerations in this plot. The two most important reasons for this are that the impact velocities of the water barricade in the 3-D computations are relatively low, and much of the water simply bypasses the acceptor stack without ever hitting it. Computation 2DC shows a much larger peak acceleration of 143.4 km/s2 at 1.00 ms and two deceleration peaks, the greatest of which is –19.22 km/s2 at 32.80 ms. The deceleration peaks correspond to the two-step impact process of the barricade against the acceptor stack left surface [15]. Computation 2DUa showed an acceleration peak of 125.2 km/s2 at 1.00 ms, and 2DUb shows a deceleration peak of -20.89 km/s2 at the shifted time of 31.73 ms, both very much in line with the corresponding values from 2DC.

Acceptor Stack Dynamics

Figure 17 shows the X-direction velocity of the acceptor stack versus time for all of the computations. The plots of X-direction velocity for the acceptor stack partially illustrate the building of the numerical instabilities in the iron rectangle representing the acceptor stack in the 3-D computations 3DC and 3DU. This is shown by the high-frequency signal in the black line for 3DC, ending at 47.40 ms, and later in 3DU, ending at 131.4 ms. The final X-direction velocity for the combined 3-D computations is 16.07 m/s. The magenta curves labeled "10thOrdReg" are tenth-order regression fits of the two 3-D velocity curves to allow a better depiction of the underlying trends in the curves. The corresponding velocities at the ending times of the 2-D computations are 33.40 m/s for 2DC and 39.95 m/s for computation 2DUb.

The X-direction acceleration of the solid iron rectangular parallelepiped representing the acceptor stack for the 3-D computations is shown in various forms in Figure 18. The black line labeled "3DC" shows the acceleration values that were generated by simply piece-wise differentiating the velocity with respect to time for the fully coupled 3-D computation. This illustrates the growing instability in the simulated acceptor stack, very likely caused by undamped stress waves operating in some type of feedback mode. The iron for the acceptor stack was modeled with a complete set of typical strength parameters, with no damping model. It may have been possible to reduce or eliminate this oscillatory behavior by modeling the acceptor stack as a simple hydrodynamic material. However, previous experience with trying that in other applications resulted in undesired numerical diffusion of iron into the surrounding atmosphere. Computed pressures in mixed-material cells of this type (i.e., highly compressible gas and solids with minimal compressibility) can be relatively unreliable compromises. Because a primary goal of the computation was to obtain estimates of pressure on the

acceptor stack, this way of modeling the stack was not tried. After repeated attempts to continue computation 3DC beyond 47.40 ms, the point at which the computation halted, the uncoupled computation was started. The acceleration versus time for that computation is shown with the dark blue line labeled "2DU." It also experienced the same type of stability problems in the acceptor stack, as illustrated by the oscillatory behavior, especially between 80 and 120 ms before halting at 131.74 ms. The oscillations in the acceleration histories for 3DC and 3DU in Figure 18 are so great that the underlying trends in acceleration are almost completely suppressed in the ordinate scaling of the plot.

The acceleration data shown in Figure 18 were processed in a variety of ways to bring out those underlying trends. The red line shows a 20-point rolling average of the acceleration of the acceptor stack for both computations. Also shown are a 40-point (orange line), a 75-point (magenta line), and a 100-point (cyan line) rolling average for the computations, each plotted in succession and therefore partially masking the previously plotted lines. The final plot (green line) is a separate tenth-order regression of the acceleration for each computation. Because of the wide range of the oscillations of the unmodified acceleration data, these processed-data lines are too suppressed by the scale of the ordinate to be very informative. They are presented in Figure 18 primarily to place their plotting with their own relevant scale in Figure 19 in proper perspective. There is a clear trend in the plots of running averages in Figure 19 toward bringing out the underlying acceleration history of the acceptor stack by increasing the number of points in the running averages for computations 3DC and 3DU. As would be expected, there are essentially no bulk accelerations of the acceptor stack in the negative X direction, except for a brief period after the initial air shock diffracts over and around the acceptor stack, is relieved on the left face, and loads the right face. The tenth-order regressions for the computations illustrate a disjoint nature at the temporal boundary between the two computations at 47.40 ms. The downward direction of the tenth-order regression for 3DC at that time is a typical artifice of the end of the range of a high-order regression and has no intrinsic physical meaning.

Figure 20 shows a comparative set of X-direction acceleration plots for the acceptor stack for the 2-D and 3-D computations. Only the 100-point running averages and the tenth-order regressions are shown for the 3-D computations. The greatest acceleration values in these processed plots are approximately 1.0 km/s2. The fully coupled 2-D computation 2DC (cyan line) shows a peak acceleration of 9.28 km/s2 at 32.80 ms, and the uncoupled 2-D computation pair (the disjoint green lines) shows a peak acceleration of 10.34 km/s2 at 31.72 ms.

Figure 21 shows the average overpressure on the left surface of the acceptor stack for the 3-D computations, computed by taking an unweighted average of pressure at 420 equally spaced points covering that surface. The black line is for 3DC,

with the average pressure from the air shock represented by the double peak of about 0.7 MPa occurring between 4 and 10 ms, and a separate peak of about 1.05 MPa at 26.0 ms. The second peak at 26.0 ms is caused by the beginning of the impact of water from the barricade on the acceptor stack. The greatest average pressure of 5.02 MPa occurs at 69.92 ms in computation 3DU (dark blue line), corresponding to the main impact of the reconstituted trapezoidal water barricade against the left surface of the acceptor stack. The average overpressure on the left surface of the acceptor stack returned to nearly atmospheric by the ending time of 3DU. This is consistent with the very low X-direction acceleration at that time, shown in Figure 20. The average pressure on the acceptor stack left surface is shown only for the 3-D computations in Figure 21 so that their dynamic features may be seen in an ordinate scale tailored for those values.

The average pressure on the left surface of the acceptor stack for all computations is shown in Figure 22. This includes the results for computations 3DC and 3DU that are in Figure 21, now shown in a plotting scale dominated by the results from the 2-D computations. The fully coupled 2-D computation, 2DC, has a peak average pressure of 38.90 MPa at 32.83 ms, 7.75 times the peak average pressure for 3DU. The uncoupled 2-D computation, 2DUb, has a greater peak average overpressure of 49.96 MPa at 31.59 ms compared with 2DC and is 9.95 times that for 3DU. Uncoupling the 2-D computations resulted in computing a greater peak average overpressure on the left surface of the acceptor stack [15]. Although the conclusion does not follow with certainty, this at least indicates a reasonable probability that the necessary uncoupling of the 3-D computations resulted in overpredicting, rather than underpredicting, the average overpressure on the left surface of the acceptor stack.

While the bulk motion of the acceptor stack is primarily a function of the average overpressure on the left surface, the maximum pressure experienced by any given munition is extremely important. Figure 23 shows plots of both the average overpressure on the acceptor stack left surface and the maximum overpressure for each point in time experienced at any of the 420 points on that surface for computations 3DC and 3DU. The maximum overpressure on the acceptor stack left surface in 3DC is 48.80 MPa at 24.23 ms, and the maximum for 3DU is 45.84 MPa at 69.90 ms, both relatively low values compared with the direct-shock initiation criteria suggested by Liddiard and Forbes [3].

For comparison, the average and maximum overpressures on the acceptor stack left face for all of the 2-D computations are shown in Figure 24. The maximum pressure for computation 2DC is 233.7 MPa (2.34 kbar) at 16.94 ms, and the maximum for the second of the uncoupled pair of computations, 2DUb, is 486.8 MPa (4.87 kbar) at 28.29 ms. The 4.87-kbar overpressure is in excess of the shock initiation criteria suggested by Liddiard and Forbes [3]. These peak values are several times less than those shown for the 3-D computations in Figure 23,

none of which indicated a possible shock initiation of the explosives in the acceptor stack in the 3-D simulations. Figure 25 shows a combined set of average and maximum overpressure plots for the 3-D computations, 3DC and 3DU, and the fully coupled 2-D computation, 2DC. The results for 2DUa and 2DUb were not included simply because their inclusion would have both dominated the scaling of the ordinate and produced too much overwriting of plots below the 20-MPa overpressure level to allow Figure 25 to be particularly informative.

CONCLUSION

The 3-D computations showed maximum overpressures on the acceptor stack left face that were six to eight times less than those suggested by Liddiard and Forbes [3] to be necessary for direct initiation by shock. It was necessary to perform the 3-D computations in two stages, the first in a fully coupled mode (3DC) and the second in an uncoupled mode (3DU). Comparisons with previous 2-D computations [5, 15] were made to address the nature of the probable error and uncertainty caused by this uncoupling. The overpressures computed in the fully coupled 2-D computation [15] had previously been shown to be significantly less than those computed in the uncoupled 2-D computations [5]. By inference, it could be reasonably concluded, but not proven with certainty, that the overpressures on the acceptor stack left face in 3DU were most probably higher than would have been computed in a fully coupled 3-D computation which had run to completion. The actual experiment [22] involving a mirror-image layout of the worst-case acceptor stacks protected by a three-bag water barricade from a command-detonated donor stack resulted in a delayed-reaction ignition and detonation of one of the acceptor stacks. It appeared that the ignition of that acceptor stack began in the vicinity of the bottom-rear of the stack at relatively late time, after the stack had translated along the ground plane for some reasonably significant distance. Because of the dust and debris, accurate determination of those important details was not possible from the limited video and instrumentation records. The originating event could have been some combination of shearing, crushing, and munition-on-munition impact [3,4]. Aspects of this were explored in previous ARL technical reports [19, 20].

The implication of this and the previous ARL technical reports on the protection offered by various water barricade configurations [5, 15-22] relative to obtaining relief from quantity-distance guidelines [1] for temporary storage of munitions during military operations is somewhat unclear. This work has provided significant support for an argument that a relatively massive water barricade can provide sufficient protection to prevent direct-shock initiation of an acceptor stack. However, this is at best a necessary, but not sufficient condition on which a decision can be made. The barricade in these studies was made of water, but that may not be necessarily so in actual practice for practical reasons. The computations, though technically complex and difficult, were all for highly

simplified, high-order detonations of a condensed, uncased explosive charge with the barricade and acceptor stack modeled as simple, continuous structures. In an actual event, the donor stack might react in a series of discrete burning, explosion, and detonation events over an extended period, with the attendant production of firebrands, burning and possibly propelled munitions, and progressive destruction of protective barricades.

ACKNOWLEDGMENTS

Technical consultation on the selection of munitions to be modeled was provided by Drs. Robert Frey and John Starkenberg of the U.S. Army Research Laboratory (ARL). Technical consultation and support in the use of the latest versions of the CTH hydrodynamics computer code were provided by Messrs. Stephen Schraml and Kent Kimsey of ARL and by Dr. Eugene Hertel of Sandia National Laboratories, New Mexico. Technical and financial support were provided by Mr. Duane Scarborough of the U.S. Army Defense Ammunition Logistics Activity, Picatinny Arsenal, New Jersey. The technical review of this report was provided by Dr. John Starkenberg of ARL. The assistance and support of all these people are gratefully acknowledged.

REFERENCES

1. "DoD Explosives Safety Board (DDESB), and DoD Component Explosives Safety Responsibilities," DoD Directive 6055.9, July 1999.

2. K.C. O'Heran, "Explosives Safety Storage Criteria for Combat and Contingencies," Proceedings 28th DOD Explosives Safety Seminar, Orlando, FL, 18-20 August 1998.

3. T.P. Liddiard and J.W. Forbes, *A Summary Report of the Modified Gap Test and the Underwater Sensitivity Test*," tech. report NSWC TR-86-350, Naval Surface Warfare Center, Silver Spring, MD, 12 March 1987.

4. T.P. Liddiard, Jr., "The Initiation of Burning in High Explosives by Shockwaves," Fourth Symposium (International) on Detonation, White Oak, MD, 12-15 October 1965.

5. R.E. Lottero, *Responses of a Water Barricade and an Acceptor Stack to the Detonation of a Donor Munitions Stack*, tech. report ARL-TR-1600, U.S. Army Research Laboratory, Aberdeen Proving Ground, MD, March 1998.

6. J.M. McGlaun et al., *A Brief Description of the Three-Dimensional Shock Wave Physics Code CTH*, tech. report SAND 89-0607, Sandia National Laboratories, Albuquerque, NM, July 1990.

7. R.L. Bell et al., "CTHGEN User's Manual and Input Instructions, Version 3.00," CTH Development Project, Sandia National Laboratories, Albuquerque, NM, 18 July 1996.

8. R.L. Bell et al., "CTH User's Manual and Input Instructions, Version 3.00," CTH Development Project, Sandia National Laboratories, Albuquerque, NM, 18 July 1996.

9. Headquarters, Department of the Army, *Technical Manual. Army Ammunition Data Sheets. Artillery Ammunition. Guns, Howitzers, Mortars, Recoilless Rifles, Grenade Launchers, and Artillery Fuzes*, tech. manual TM-43-0001-28, Washington, DC, April 1977.

10. J. Starkenberg, K.J. Benjamin, and R.B. Frey, *Predicting Fragmentation Propagation Probabilities for Ammunition Stacks*," tech. report ARL-TR-949, U.S. Army Research Laboratory, Aberdeen Proving Ground, MD, January 1996.

11. Federal Fabrics-Fibers, Inc., "Rapid Ammunition Barricade Technology Development, Small Business Innovative Research Contract DAAE30-97-C-1023, 10 March 1997.

12. R.E. Lottero, "Numerical Modeling of the Responses of a Water Barricade and an Acceptor Stack to the Detonation of a Donor Munitions Stack," Proceedings of the 28th DDESB Explosives Safety Seminar, Orlando, FL, 18-20 August 1998.

13. R.L. Bell, et al., "CTHGEN User's Manual and Input Instructions, Version 4.00," CTH Development Project, Sandia National Laboratories, Albuquerque, NM, 10 March 1998.

14. R.L. Bell et al., "CTH User's Manual and Input Instructions, Version 4.00." CTH Development Project, Sandia National Laboratories, Albuquerque, NM, 13 March 1998.

15. R.E. Lottero, *Standoff Variation Study I: Detonation of a Donor Munitions Stack and Responses of a Trapezoidal Water Barricade and an Acceptor Stack,* tech. report ARL-TR-1943, U.S. Army Research Laboratory, Aberdeen Proving Ground, MD, May 1999.

16. R.E. Lottero, *Standoff Variation Study II: Detonation of a Donor Munitions Stack and Responses of a Thin Rectangular Water Barricade and an Acceptor Stack,* tech. report ARL-TR-1948, U.S. Army Research Laboratory, Aberdeen Proving Ground, MD, May 1999.

17. R.E. Lottero, *Standoff Variation Study III: Detonation of a Donor Munitions Stack and Responses of a Thick Rectangular Water Barricade and an Acceptor Stack*, tech. report ARL-TR-2035, U.S. Army Research Laboratory, Aberdeen Proving Ground, MD, August 1999.

18. R.E. Lottero, "A Computational Study of the Responses to the Detonation of a Donor Munitions Stack of a Water Barricade of Various Cross Sections and an Acceptor Munitions Stack at Various Standoffs," Proceedings 29th DDESB Explosives Safety Seminar, New Orleans, LA, 18-20 July 2000.

19. O. Lyman, R. Frey, and W. Lawrence, *Determination of a Worst-Case Acceptor for Large-Scale Sympathetic Detonation Testing*, tech. report ARL-TR-490, U.S. Army Research Laboratory, Aberdeen Proving Ground, MD, July 1994.

20. P.B. Simmers and R.E. Lottero, *A Computational Study of Munitions Response to Double Impact and Crushing Impact From a Flyer Plate*, tech. report ARL-TR-2279, U.S. Army Research Laboratory, Aberdeen Proving Ground, MD, August 2000.

21. R.E. Lottero and P. B. Simmers, "Hydrocode Computations of the Responses of M2A3 and M483 Munitions to Double Impact and Crushing Impact From a Flyer Plate," Proceedings 29th DDESB Explosives Safety Seminar, New Orleans, LA, 18-20 July 2000.

22. J.D. Sullivan, J. Starkenberg, and J. L. Brown, *Water Bag and Concertainer Detonation Barricades*, tech. report ARL-TR-2330, U.S. Army Research Laboratory, Aberdeen Proving Ground, MD, September 2000.

23. B.M. Dobratz, and P.C. Crawford, *LLNL Explosives Handbook, Properties of Chemical Explosives and Explosive Simulants*, tech. report UCRL-52997, Change 2, Lawrence Livermore National Laboratory, Livermore, CA, 31 January 1985.

24. G.I. Kerley, *CTH Reference Manual: The Equation of State Package*, tech. report SAND 91-0344, Sandia National Laboratories, Albuquerque, NM, 24 May 1991.

25. F.H Ree, *Equation of State for Water*, tech. report UCRL-52190, Lawrence Livermore National Laboratory, Livermore, CA, December 1976.

FIGURE CAPTIONS

Figure 1. A 2-D cut at Y = 2.00 cm (elevation view) in the flow field in computation 3DC at time = 0.00.

Figure 2. A 2-D cut at Z = 2.00 cm (plan view) in the flow field in computation 3DC at time = 0.00.

Figure 3. A 2-D cut at Y = 2.00 cm (elevation view) in the flow field in computation 3DC at time = 47.40 ms.

Figure 4. A 2-D cut at Z = 2.00 cm (plan view) in the flow field in computation 3DC at time = 47.40 ms.

Figure 5. A 2-D cut at Y = 2.00 cm (elevation view) in the flow field in computation 3DU at time = 47.40 ms.1

Figure 6. A 2-D cut at Z = 2.00 cm (plan view) in the flow field in computation 3DU at time = 47.40 ms.

Figure 7. A 2-D cut at Y = 2.00 cm (elevation view) in the flow field in computation 3DU at time = 131.74 ms.

Figure 8. A 2-D cut at Z = 2.00 cm (plan view) in the flow field in computation 3DU at time = 131.74 ms.

Figure 9. The flow field in computation 2DC at time = 0.00.

Figure 10. The flow field in computation 2DC at time = 40.00 ms.

Figure 11. The flow field in computation 2DUa at time = 0.00.

Figure 12. The flow field in computation 2DUa at time = 8.00 ms.

Figure 13. The flow field in computation 2DUb at time = 0.00.

Figure 14. The flow field in computation 2DUb at time = 7.80 ms.

Figure 15. The barricade X-direction velocity for all computations.

Figure 16. The barricade X-direction acceleration for all computations.

Figure 17. The acceptor stack X-direction velocity for all computations.

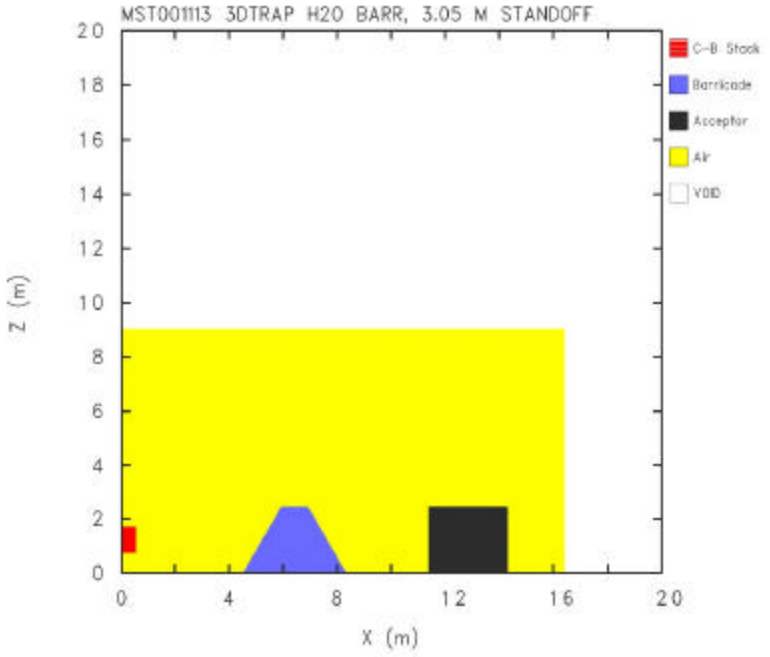

Figure 1. A 2-D cut at Y = 2.00 cm (elevation view) in the flow field in computation 3DC at time = 0.00.

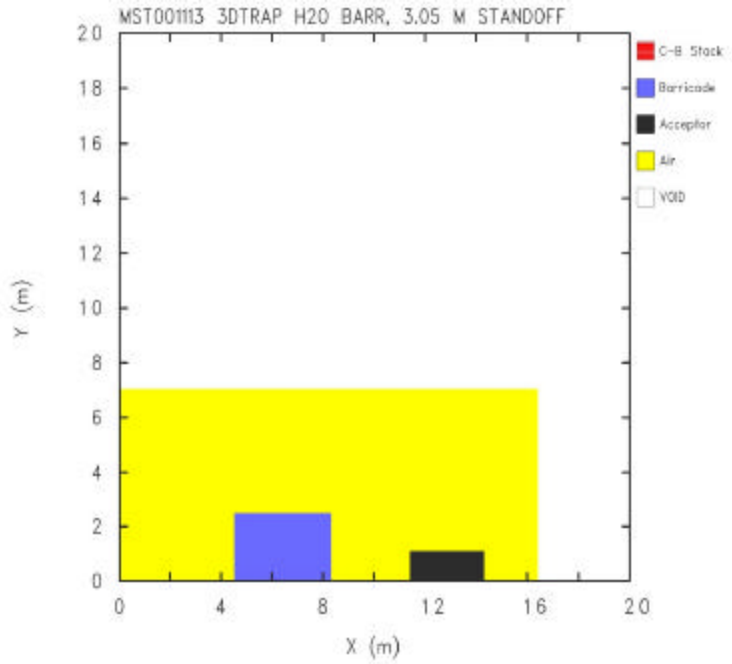

Figure 2. A 2-D cut at Z = 2.00 cm (plan view) in the flow field in computation 3DC at time = 0.00.

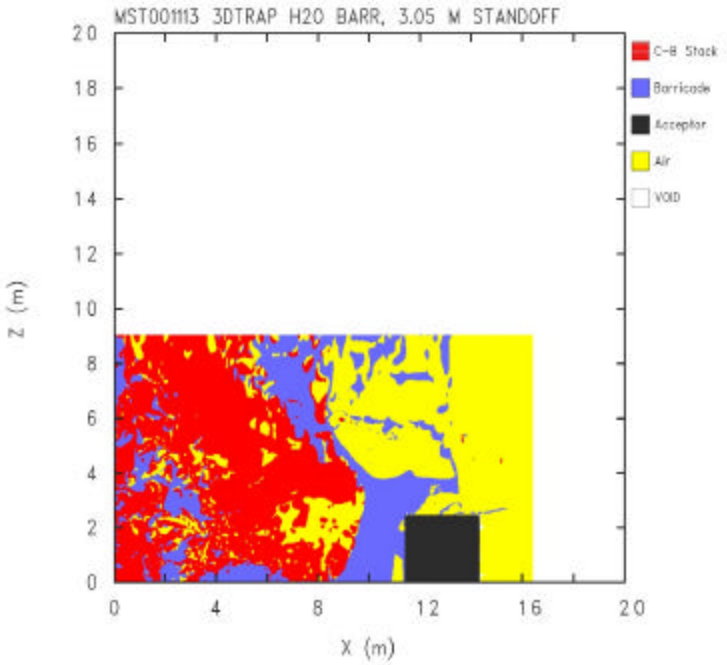

Figure 3. A 2-D cut at Y = 2.00 cm (elevation view) in the flow field in computation 3DC at time = 47.40 ms.

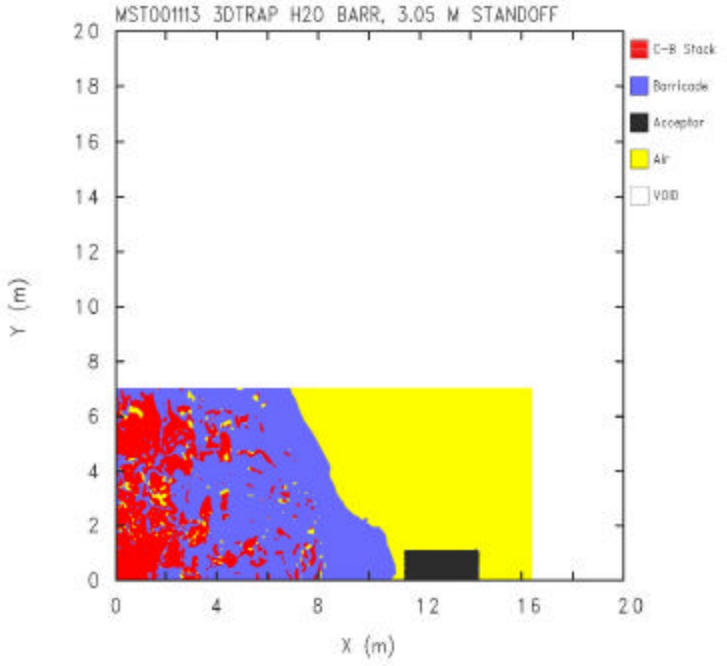

Figure 4. A 2-D cut at Z = 2.00 cm (plan view) in the flow field in computation 3DC at time = 47.40 ms.

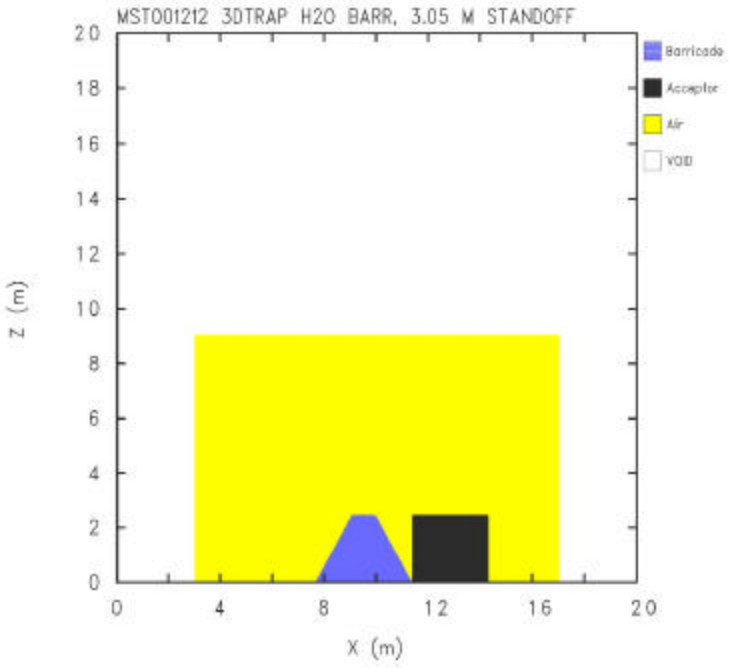

Figure 5. A 2-D cut at Y = 2.00 cm (elevation view) in the flow field in computation 3DU at time = 47.40 ms.

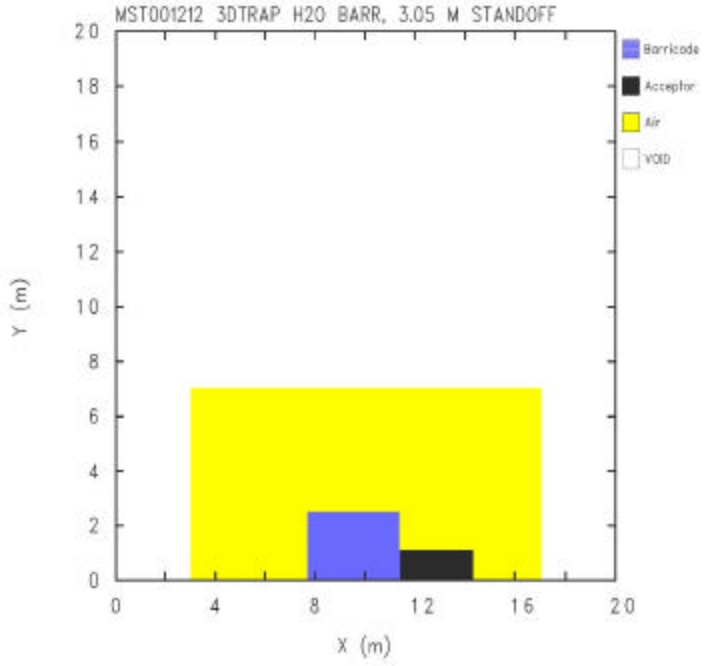

Figure 6. A 2-D cut at Z = 2.00 cm (plan view) in the flow field in computation 3DU at time = 47.40 ms.

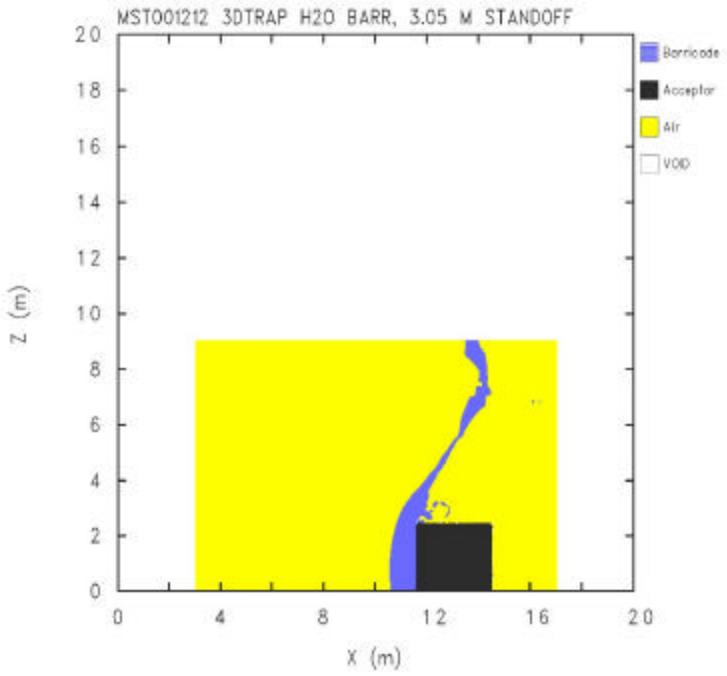

Figure 7. A 2-D cut at Y = 2.00 cm (elevation view) in the flow field in computation 3DU at time = 131.74 ms.

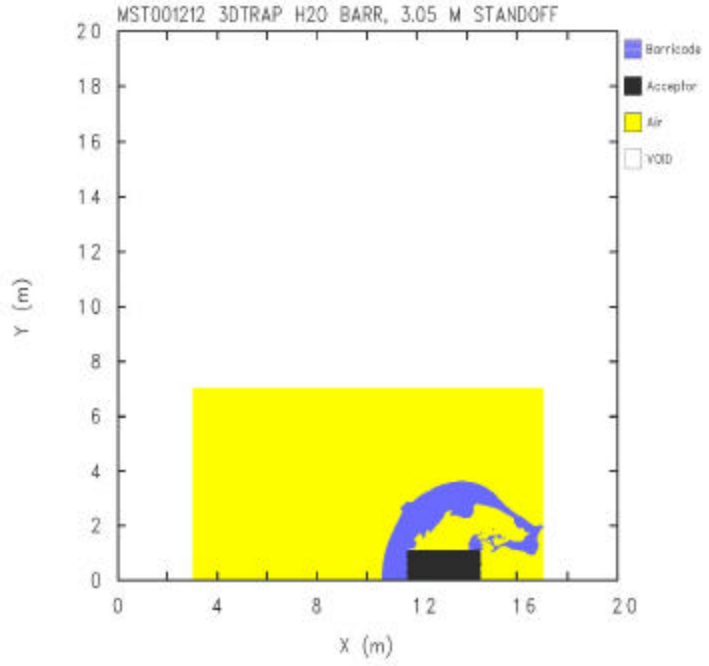

Figure 8. A 2-D cut at Z = 2.00 cm (plan view) in the flow field in computation 3DU at time = 131.74 ms.

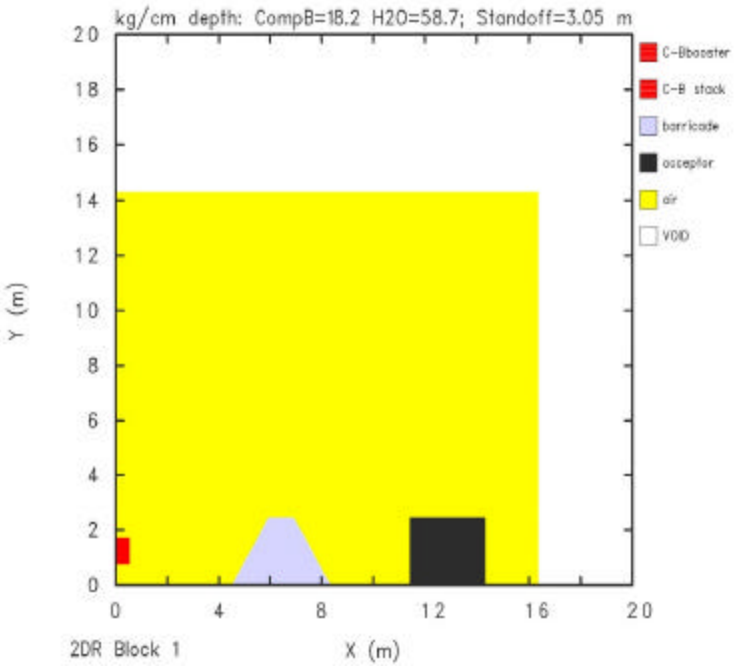

Figure 9. The flow field in computation 2DC at time = 0.00.

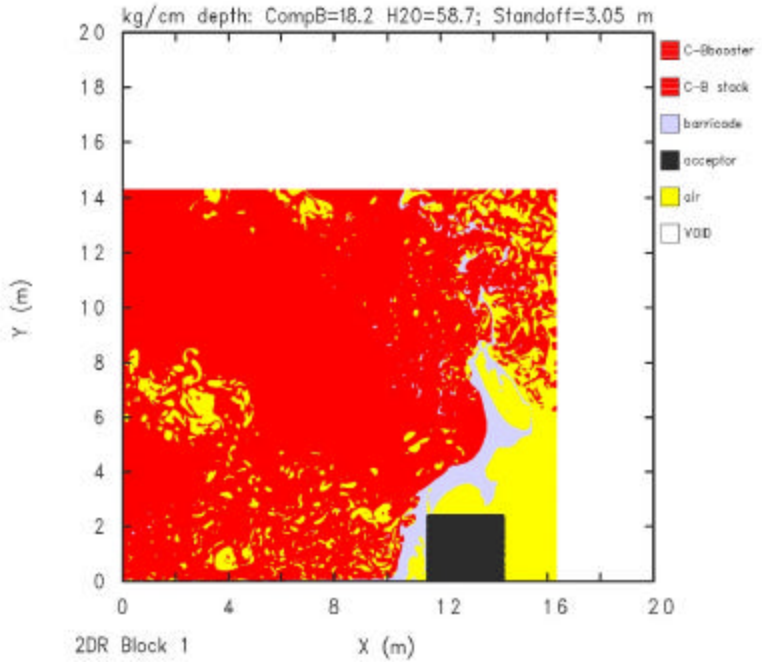

Figure 10. The flow field in computation 2DC at time = 40.00 ms.

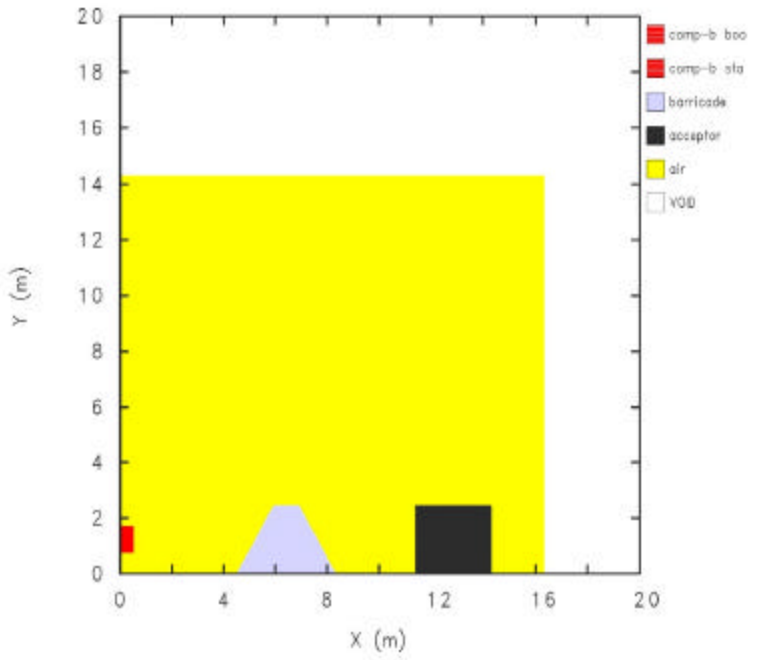

Figure 11. The flow field in computation 2DUa at time = 0.00.

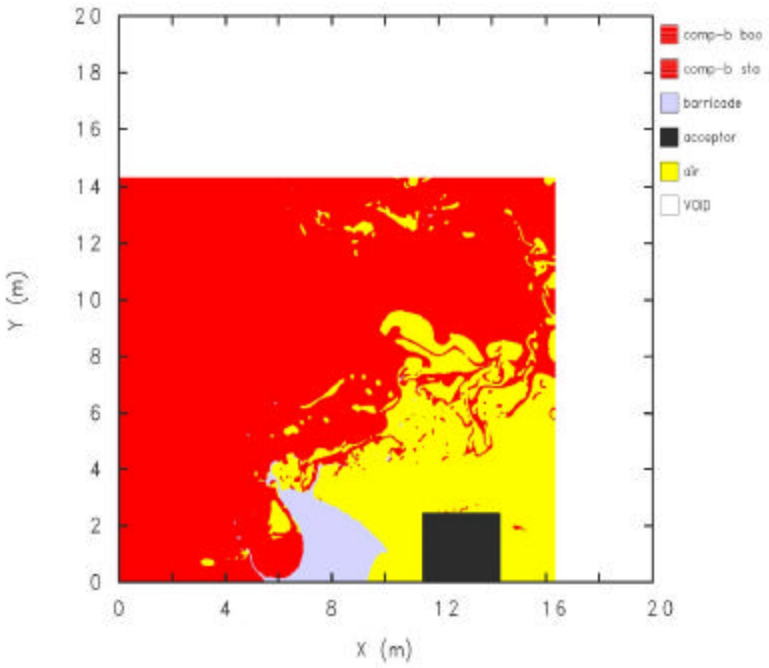

Figure 12. The flow field in computation 2DUa at time = 8.00 ms.

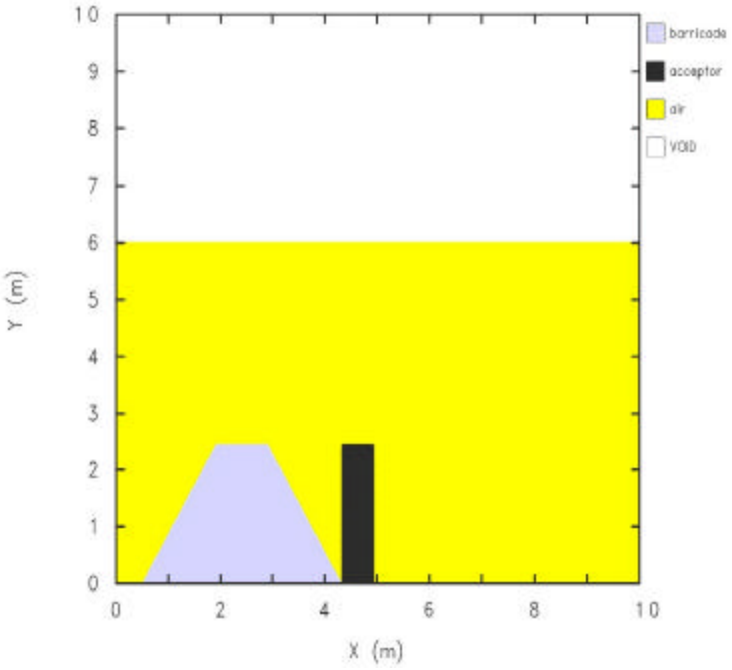

Figure 13. The flow field in computation 2DUb at time = 0.00.

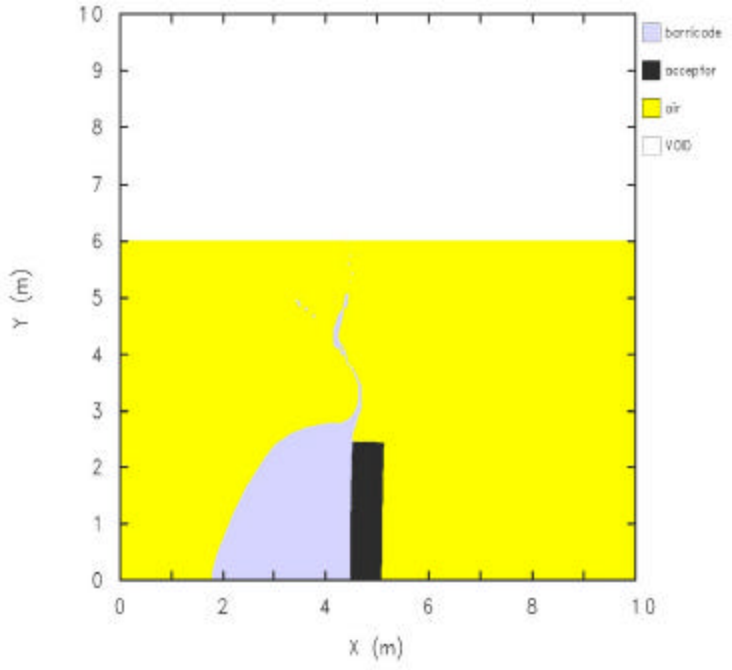

Figure 14. The flow field in computation 2DUb at time = 7.80 ms.

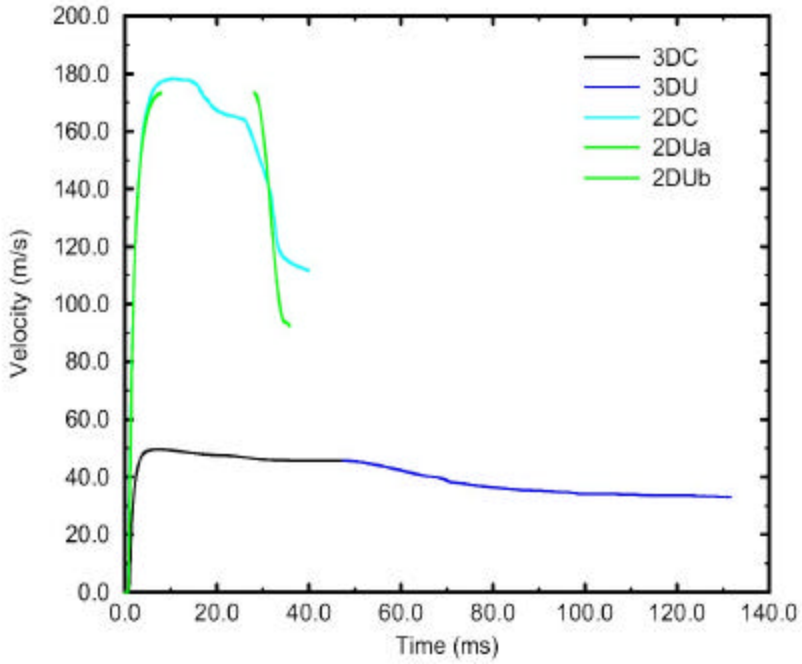

Figure 15. The barricade X-direction velocity for all computations.

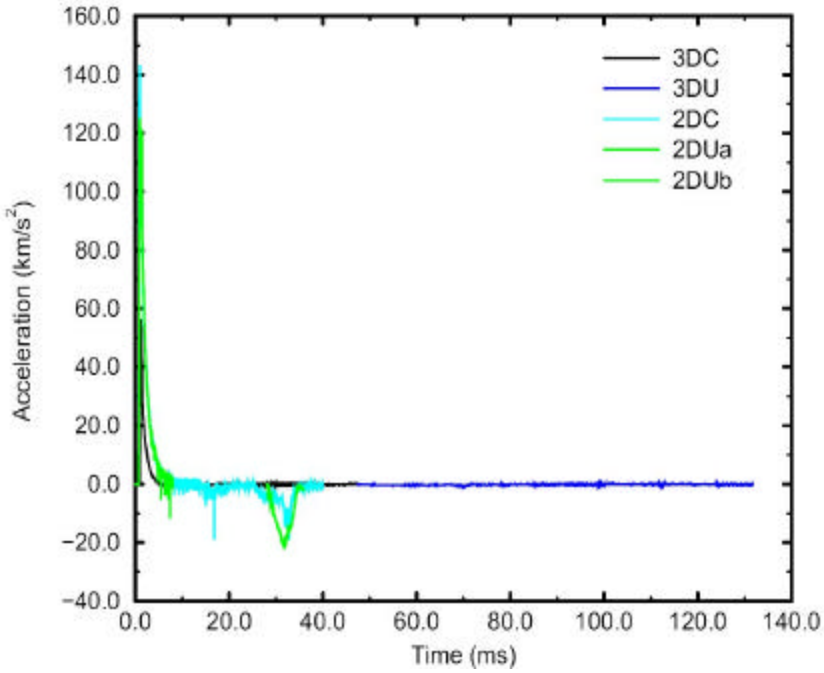

Figure 16. The barricade X-direction acceleration for all computations.

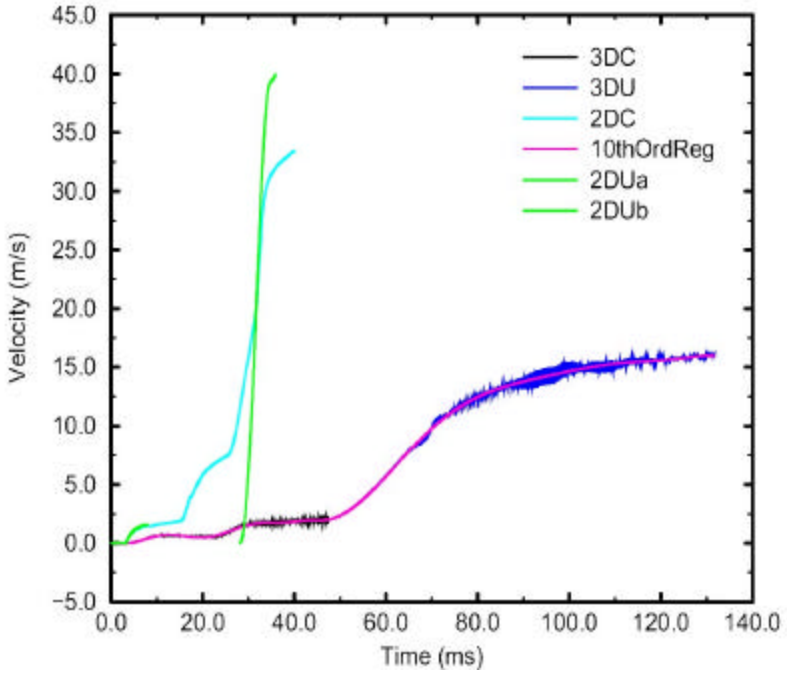

Figure 17. The acceptor stack X-direction velocity for all computations.

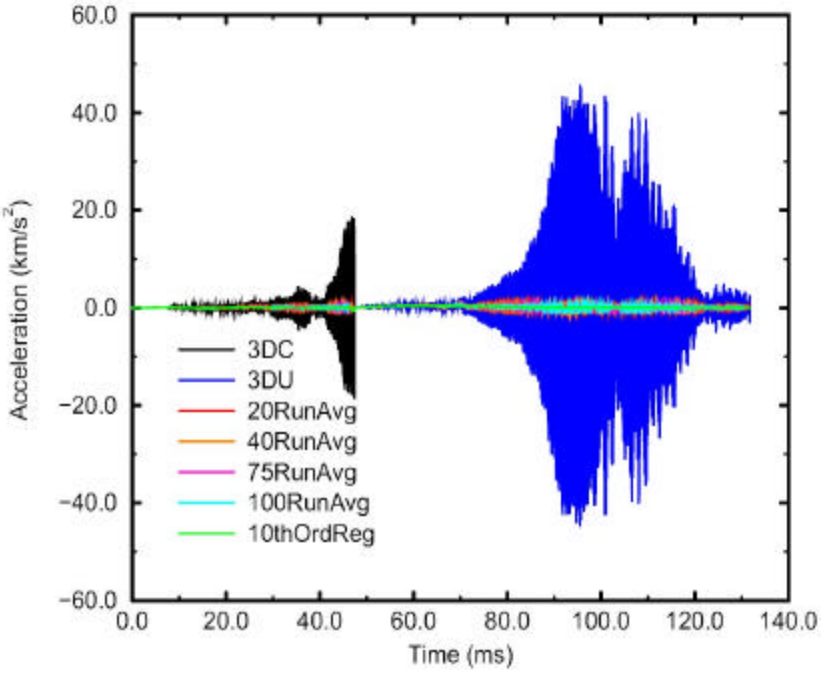

Figure 18. The acceptor stack X-direction acceleration for the 3-D computations, including various running averages and tenth-order regressions.

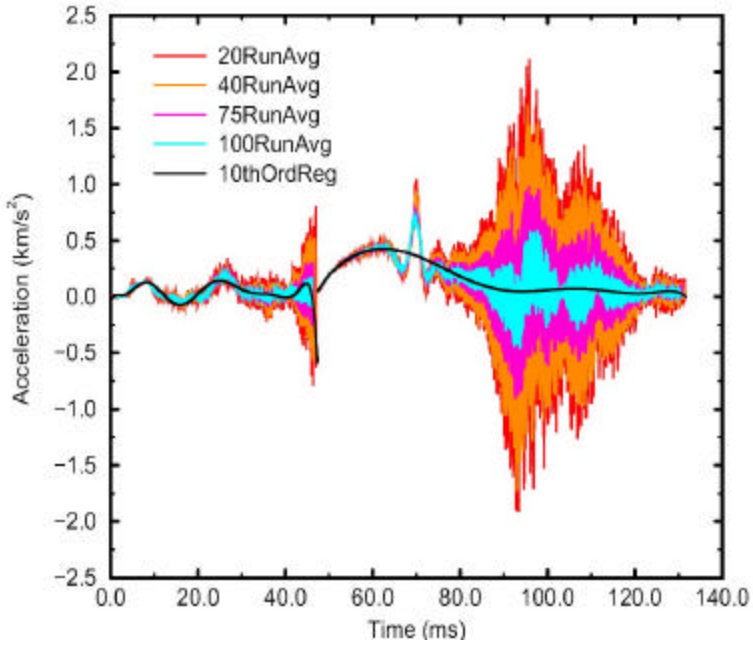

Figure 19. The acceptor stack X-direction acceleration for the 3-D computations, showing only running averages and the tenth-order regressions.

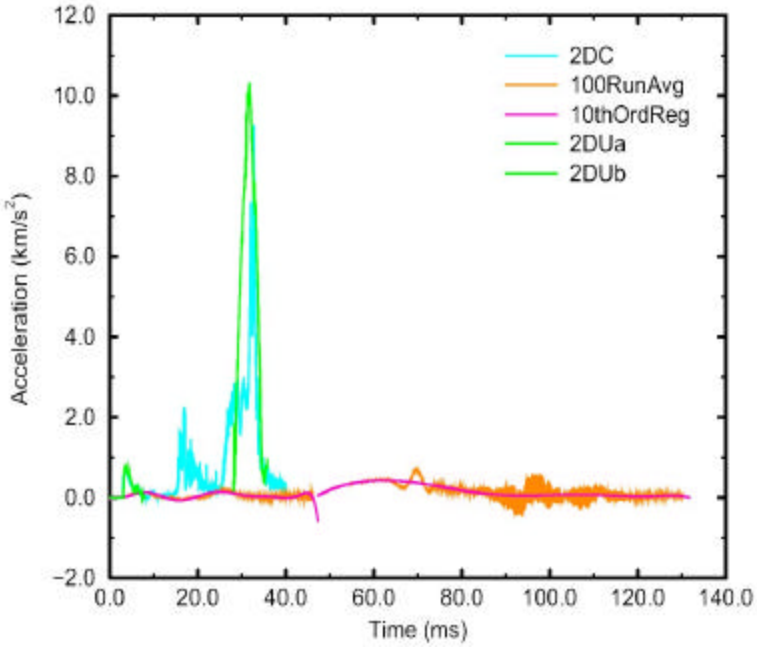

Figure 20. The acceptor stack X-direction acceleration for the 2-D computations, and the 100-point running averages and tenth-order regressions for the 3-D computations.

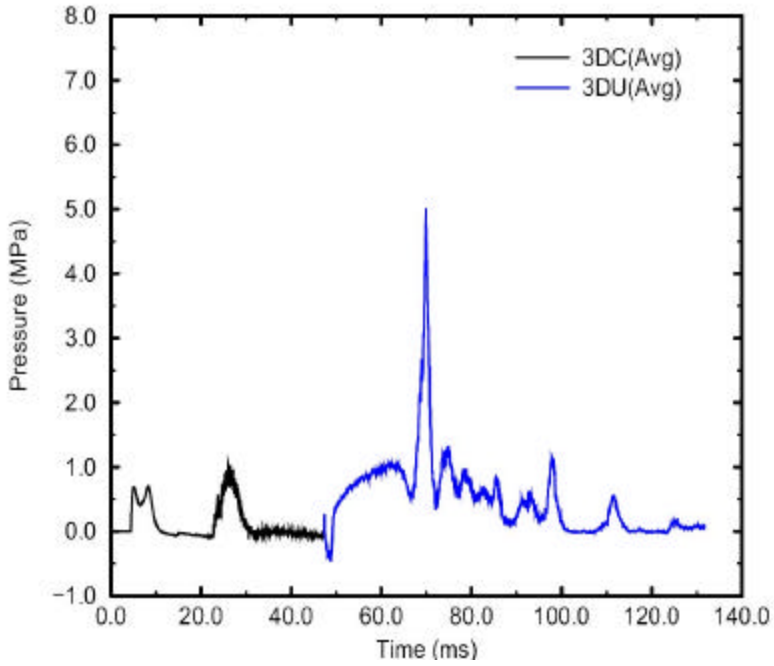

Figure 21. Average overpressure on the acceptor stack left surface for the 3-D computations.

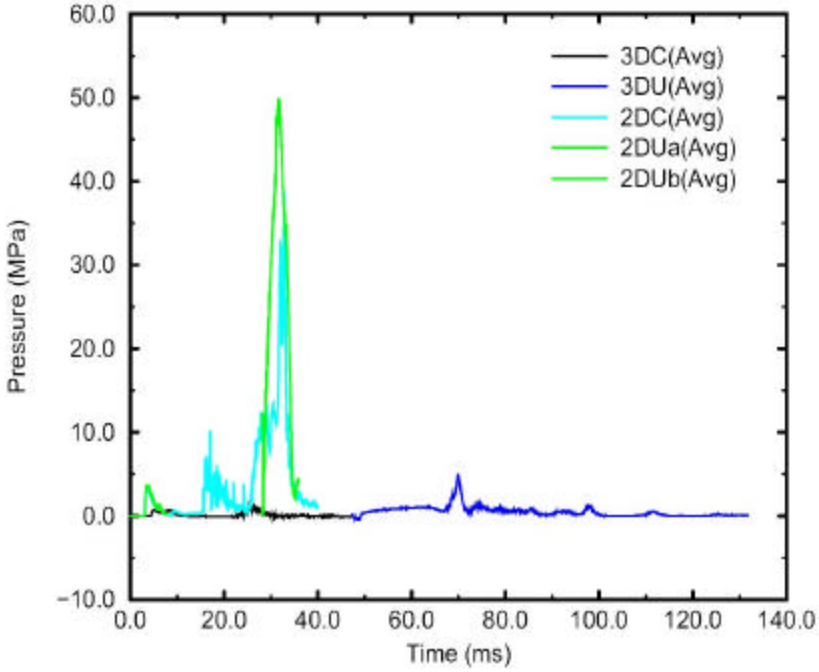

Figure 22. Average overpressure on the acceptor stack left surface for all computations.

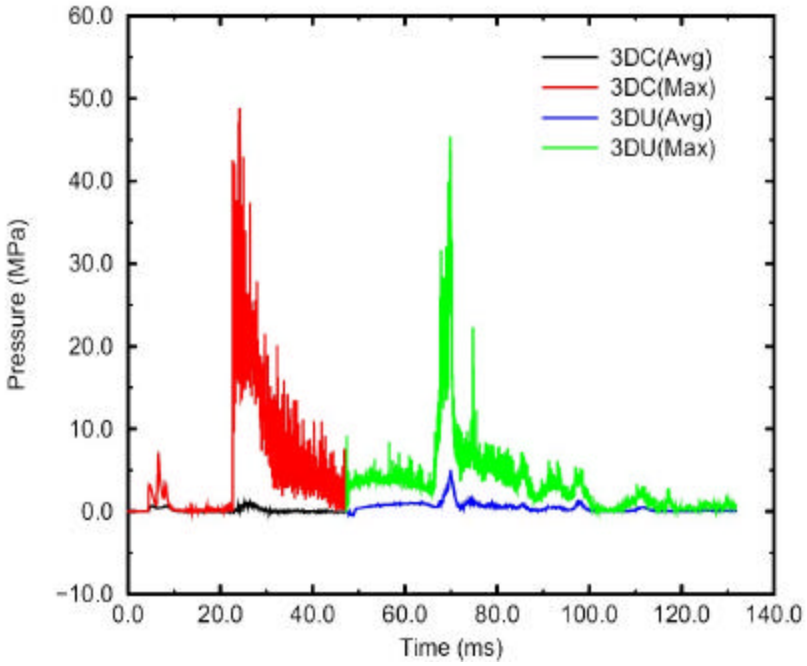

Figure 23. Average and maximum overpressure on the acceptor stack left surface for the 3-D computations.

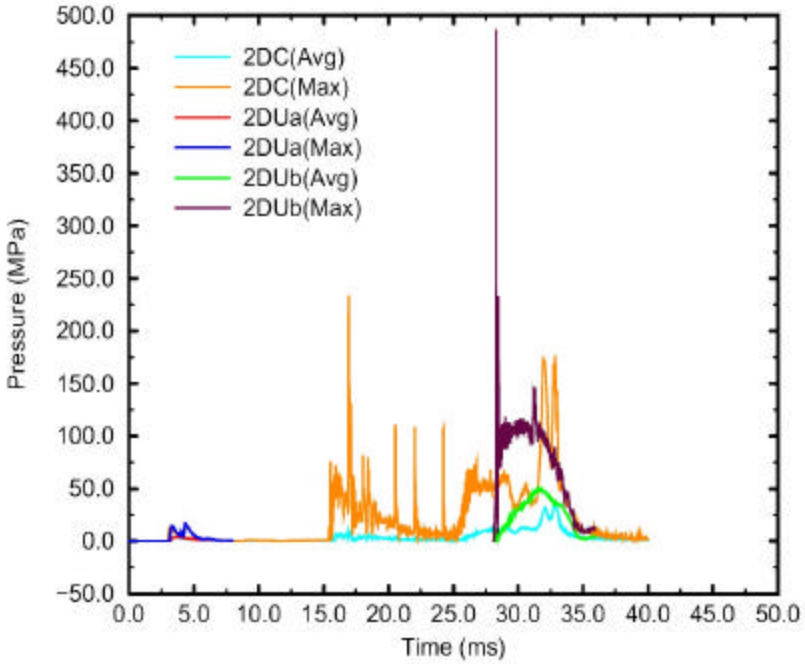

Figure 24. Average and maximum overpressure on the acceptor stack left surface for the 2-D computations.

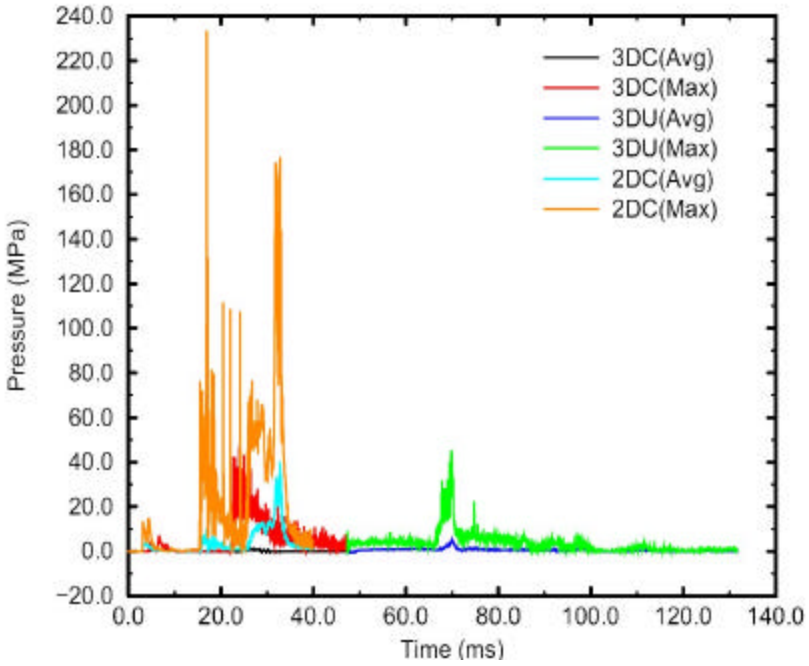

Figure 25. Average and maximum overpressure on the acceptor stack left surface for the 3-D and the 2-D fully coupled computations.